Design and Development of ^{99m}Tc-Labeled FAPI Tracers for SPECT Imaging and ^{188}Re Therapy

Thomas Lindner[1], Annette Altmann[1,2], Susanne Krämer[1], Christian Kleist[1], Anastasia Loktev[1,2], Clemens Kratochwil[1], Frederik Giesel[1], Walter Mier[1], Frederik Marme[3], Jürgen Debus[4,5], and Uwe Haberkorn[1,2,6]

[1]Department of Nuclear Medicine, University Hospital Heidelberg, Heidelberg Germany; [2]Clinical Cooperation Unit Nuclear Medicine, German Cancer Research Center (DKFZ), Heidelberg, Germany; [4]Department of Radiation Oncology, University Hospital Heidelberg, Heidelberg, Germany; [5]Clinical Cooperation Unit Radiation Oncology, German Cancer Research Center (DKFZ), Heidelberg, Germany; [3]Translational Gynecologic Oncology, University Hospital Mannheim, Mannheim, Germany; and [6]Translational Lung Research Center Heidelberg, German Center for Lung Research (DZL), Heidelberg, Germany

Most epithelial tumors recruit fibroblasts and other nonmalignant cells and activate them into cancer-associated fibroblasts. This often leads to overexpression of the membrane serine protease fibroblast-activating protein (FAP). It has already been shown that DOTA-bearing FAP inhibitors (FAPIs) generate high-contrast images with PET/CT scans. Since SPECT is a lower-cost and more widely available alternative to PET, ^{99m}Tc-labeled FAPIs represent attractive tracers for imaging applications in a larger number of patients. Furthermore, the chemically homologous nuclide ^{188}Re is available from generators, which allows FAP-targeted endoradiotherapy. **Methods:** For the preparation of ^{99m}Tc-tricarbonyl complexes, a chelator was selected whose carboxylic acids can easily be converted into various derivatives in the finished product, enabling a platform strategy based on the original tracer. The obtained ^{99m}Tc complexes were investigated in vitro by binding and competition experiments on FAP-transfected HT-1080 (HT-1080-FAP) or on mouse FAP-expressing (HEK-muFAP) and CD26-expressing (HEKCD26) HEK cells and characterized by planar scintigraphy and organ distribution studies in tumor-bearing mice. Furthermore, a first-in-humans application was done on 2 patients with ovarian and pancreatic cancer, respectively. **Results:** ^{99m}Tc-FAPI-19 showed specific binding to recombinant FAP-expressing cells with high affinity. Unfortunately, liver accumulation, biliary excretion, and no tumor uptake were observed on planar scintigraphy for a HT-1080-FAP–xenotransplanted mouse. To improve the pharmacokinetic properties, hydrophilic amino acids were attached to the chelator moiety of the compound. The resulting ^{99m}Tc-labeled FAPI tracers revealed excellent binding properties (≤45% binding; >95% internalization), high affinity (half-maximal inhibitory concentration, 6.4–12.7 nM), and significant tumor uptake (≤5.4% injected dose per gram of tissue) in biodistribution studies. The lead candidate ^{99m}Tc-FAPI-34 was applied for diagnostic scintigraphy and SPECT of patients with metastasized ovarian and pancreatic cancer for follow-up to therapy with ^{90}Y-FAPI-46. ^{99m}Tc-FAPI-34 accumulated in the tumor lesions, as also shown on PET/CT imaging using ^{68}Ga-FAPI-46. **Conclusion:** ^{99m}Tc-FAPI-34 represents a powerful tracer for diagnostic scintigraphy, especially when PET imaging is not available. Additionally, the chelator used in this compound allows labeling with the therapeutic nuclide ^{188}Re, which is planned for the near future.

Key Words: fibroblast activating protein; SPECT; theranostics; small molecule inhibitor

J Nucl Med 2020; 61:1507–1513
DOI: 10.2967/jnumed.119.239731

Although in the classic approach mainly tumor cells were the sole target for cancer therapy, the tumor microenvironment and tumor stroma came increasingly into focus to enable novel forms of treatment. Cancer-associated fibroblasts are an important component in a large number of neoplasias, as they actively contribute to tissue remodeling, resistance development, and immune evasion (*1*). Cancer-associated fibroblasts can be formed from different progenitors, resulting in variations of their proteome. However, many cancer-associated fibroblasts are characterized by an overexpression of the fibroblast-activating protein (FAP) (*2,3*). This protein is a membrane-bound serine protease with both dipeptidyl peptidase and endopeptidase activity that hydrolyzes denatured collagen type 1, among other substrates. Since FAP is almost absent in healthy tissue, inhibitors of FAP (FAPIs) can be used in nuclear medicine for PET imaging and possibly also for endoradiotherapy of a variety of cancers with a desmoplastic reaction, such as pancreatic, breast, and colon carcinomas (*4–10*).

Using ^{68}Ga-labeled FAPIs for preclinical and clinical PET/CT imaging, we observed a high rate of internalization of the tracer but also considerable efflux. This resulted in relatively short intratumoral half-lives (*5,11*). For a therapeutic application of this family of compounds, the physical half-life of the radionuclide used for labeling has to be adjusted to the biologic half-life in the tumor. Therefore, ^{177}Lu and ^{225}Ac, which have been applied successfully for the targeted treatment of neuroendocrine tumors and prostate cancer, are not useful in this context. In contrast, short-lived isotopes such as the α-emitter ^{213}Bi or the β-emitter ^{188}Re may deliver higher doses to the tumor. However, whereas ^{213}Bi can be used for the molecules developed so far, labeling of FAPIs with ^{188}Re requires a different chelator coupled to the binding moiety. Chelators binding ^{188}Re could be also used for labeling with ^{99m}Tc for scintigraphy and SPECT.

Therefore, the goal of this project was 2-fold: the development of a tracer for endoradiotherapy with ^{188}Re and for widespread scintigraphic diagnostics with ^{99m}Tc.

Received Nov. 14, 2019; revision accepted Feb. 26, 2020.
For correspondence or reprints contact: Uwe Haberkorn, Department of Nuclear Medicine, University Hospital Heidelberg, Im Neuenheimer Feld 400, 69120 Heidelberg, Germany.
E-mail: uwe.haberkorn@med.uni-heidelberg.de
Published online Mar. 13, 2020.

MATERIALS AND METHODS

Reagents

All solvents and nonradioactive reagents were obtained in reagent grade from ABCR, Sigma-Aldrich, Acros Organics, or VWR and were used without further purification. (*S*)-*N*-(2-(2-cyano-4,4-difluoropyrrolidin-1-yl)-2-oxoethyl)-6-(3-(4-*tert*-butoxycarbonylpiperazin-1-yl)-1-propoxy)quinoline-4-carboxamide was synthesized as already described (*5*). The chelator bis((1-(2-(tert-butoxy)-2-oxoethyl)1H-imidazol-2-yl) methyl)glycine was synthesized according to a method by Lu et al. (*12*) using hydrogen over 5% palladium/carbon in methanol for the reductive amination step. ^{99m}Tc was eluted from a ^{99}Mo/^{99m}Tc generator purchased from CIS bio. Human serum was obtained from Sigma-Aldrich.

Synthesis and Radiolabeling

A detailed description of the synthetic pathway and protocols can be found in the supporting information (Supplemental Fig. 1; supplemental materials are available at http://jnm.snmjournals.org). Labeling was performed with 100–150 MBq of Na[^{99m}TcO$_4$] in 1 mL of 0.9% saline, which was added to a CRS kit for tricarbonyl complexes (PSI). The mixture was heated to 95°C for 20 min to provide the intermediate [^{99m}Tc(H$_2$O)$_3$(CO)$_3$]$^+$ complex. After being cooled to room temperature, 200 μL of the solution were added to a mixture of 5 μL of the individual precursor (1 mM in water), 30 μL of phosphate buffer (0.4 M; pH 7.4), and 45 μL of hydrochloric acid (1 M), resulting in a pH of 5–6. The reaction was heated to 95°C for 20 min, and completeness was checked by radio-high-performance liquid chromatography (HPLC). The ^{99m}Tc-labeled tracers (~250–500 nmol/GBq with regard to precursor amount) were used directly for in vitro studies or processed by solid-phase extraction, evaporation, and formulation with 0.9% saline before imaging or biodistribution experiments.

Compound Analysis

Reverse-phase HPLC was conducted using linear gradients of acetonitrile in water (0%–100% acetonitrile in 5 min; 0.1% trifluoroacetic acid; flow rate, 2 mL/min) on a Chromolith Performance RP-18e column (100 × 3 mm; Merck). Ultraviolet absorbance was detected at 214 nm. An additional γ-detector was used for the HPLC analysis of radioactive compounds. HPLC–mass spectrometry characterization was performed on an ESI mass spectrometer (Exactive; Thermo Fisher Scientific) connected to an Agilent 1200 HPLC system with a Hypersil Gold C18 1.9-μm column (200 × 2.1 mm; 0%–100% acetonitrile in 20 min; flow rate, 200 μL/min). Analytical radio-HPLC was performed using a Chromolith Performance RP-18e column (100 × 3 mm [Merck]; 0%–30% acetonitrile in 10 min; flow rate, 2 mL/min). HPLC purifications were performed on a LaPrep P110 system (Knauer) and a Reprosil Pur 120 column (C18, aqueous, 5 μm, 250 × 25 mm; Dr. Maisch). The water–acetonitrile gradient (15 or 25 min; 0.1% trifluoroacetic acid; flow rate, 20 mL/min) was modified for the individual products.

Cell Culture

The binding properties of ^{99m}Tc-labeled FAPI derivatives were evaluated using HT-1080 cells stably transfected with the human FAP gene (HT-1080-FAP), as well as the mouse FAP gene (HEK-muFAP) and human CD26 (HEKCD26)–transfected human embryonic kidney cells (obtained from Stefan Bauer, NCT Heidelberg (*13*)). The cells were cultivated in Dulbecco modified Eagle's medium containing 10% fetal calf serum at 37°C and 5% carbon dioxide.

Radioligand binding studies were performed as described previously (*4,5*). In brief, recombinant cells were seeded in 6-well plates and cultivated for 48 h to a final confluence of approximately 80%–90% (1.2–2 × 10^6 cells per well). The medium was replaced by 1 mL of fresh medium without fetal calf serum. The radiolabeled compound was added to the cell culture and incubated for different intervals ranging from 10 to 240 min. Competition experiments were performed by simultaneous exposure to unlabeled (10^{-5}–10^{-10} M) and radiolabeled compound for 60 min. In all experiments, the cells were washed twice with 1 mL of phosphate-buffered saline at pH 7.4 and subsequently lysed with 1.4 mL of lysis buffer (0.3 M NaOH, 0.2% sodium dodecyl sulfate).

For internalization experiments, the cells were incubated with the radiolabeled compound for 60 and 240 min at 37°C. Cellular uptake was terminated by removing medium from the cells and washing twice with 1 mL of phosphate-buffered saline. Subsequently, the cells were incubated with 1 mL of glycine-HCl (1 M, pH 2.2) for 10 min at room temperature to harvest the surface-bound peptides (glycine fraction). Thereafter, the cells were washed with 2 mL of ice-cold phosphate-buffered saline and lysed as described (*4,5,11*) to determine the internalized (lysed) fraction. Radioactivity was determined in a Wizard γ-counter (PerkinElmer), normalized to 1 × 10^6 cells and calculated as the percentage of the applied dose. Each experiment was performed 3 times, and 3 repetitions per independent experiment were acquired.

Animal Studies

For in vivo experiments, 5 × 10^6 HT-1080-FAP cells were subcutaneously inoculated into the right trunk of 8-wk-old BALB/c *nu/nu* mice (Charles River). When the size of the tumor reached approximately 1 cm^3, the radiolabeled compound was injected via the tail vein (2–5 MBq in 100 μL of 0.9% saline for small-animal imaging and 1 MBq in 100 μL of 0.9% saline for organ distribution). For organ distribution, the animals (n = 6 or 3 for each time point) were sacrificed at 1 and 4 h or at different time points (30 min–24 h) after tracer administration. The distributed radioactivity was measured in all dissected organs and in blood using a γ-counter (Cobra Autogamma; Packard). The values are expressed as percentage injected dose per gram of tissue (%ID/g). Scintigraphic images were obtained using a γ-camera (γ-Imager; Biospace) with a recording time of 10 min per image. For the in vivo blockade experiments, 30 nmol of unlabeled FAPI were added to the radiolabeled compound directly before injection.

All animal experiments were conducted in compliance with the German animal protection laws (permission 35-91185.81/G-158/15).

Scintigraphy and SPECT/CT Imaging

The patients gave written informed consent to undergo FAPI PET/CT, FAPI therapy, and FAPI scintigraphy following the regulations of the German Pharmaceuticals Act §13(2b). All patients were referred for the experimental diagnostics by their oncologists, who were facing an unmet diagnostic challenge that could not be solved sufficiently with standard diagnostic means. The data were analyzed retrospectively with approval of the local ethics committee (approval S016/2018).

The ^{99m}Tc-FAP-34 was applied via intravenous catheter as a bolus injection of 660 MBq via a sterile filter system (Filtropur S 0.2; Sarstedt). Whole-body planar scintigraphy was performed at 10 min, 1 h, 4 h, and 20 h, and 2-bed-position SPECT/CT was performed at 4 h after tracer administration.

Scintigraphic images were obtained using a low-energy high-resolution collimating system with an acquisition time of 1 min/15 cm of body height in a 1,025 × 256 matrix. The SPECT acquisition was performed on an Infinia scanner system (GE Healthcare) using a 128 × 128 matrix, a zoom of 1, step-by-step scanning at 30 s per step, and 120 images with a 3° angle cut in a 128 × 128 matrix. For FAPI-34 imaging, a 4-slice low-dose CT scan (as a part of SPECT/CT) was performed for attenuation correction and general localization of FAPI-positive lesions.

PET/CT imaging was performed on a Biograph mCT Flow scanner (Siemens). After non–contrast-enhanced low-dose CT (130 keV, 30

mAs, CareDose; reconstructed with a soft-tissue kernel to a slice thickness of 5 mm), PET was acquired in 3-dimensional mode (matrix, 200 × 200) using FlowMotion (Siemens). The emission data were corrected for randoms, scatter, and decay. Reconstruction was performed with ordered-subset expectation maximization using 2 iterations and 21 subsets, along with Gauss filtering to a transaxial resolution of 5 mm in full width at half maximum. Attenuation correction was performed using the nonenhanced low-dose CT data. The FAPI-46 was synthesized and labeled as described previously (*11*). The injected activity for the ^{68}Ga-FAPI-46 (*11*) examinations was 260 MBq, and the PET scans began 1 h after injection. A 500-mL volume of saline with 20 mg of furosemide was infused from 15 min before to 30 min after tracer application. The patients were asked to self-report any side effects 30 min after finishing the examination.

RESULTS

Synthesis of Compounds

Detailed results of the individual synthetic steps can be found in the supporting information. An overview of FAPI-19 and corresponding FAPI derivatives is presented in Figure 1. Additionally, logP and plasma protein binding, as well as the proteolytic stability, were determined and showed similar binding for all FAPI compounds (Supplemental Table 1 (*14*)) and, exemplarily, a high stability for ^{99m}Tc-FAPI-34 over 4 h (Supplemental Fig. 2).

High Accumulation of FAPI-19 in Tumor Cells, but Unfavorable Pharmacokinetics

The first ^{99m}Tc-labeled derivative, FAPI-19, showed a binding of 35.8% ± 1.0% to 1×10^6 HT-1080-FAP cells after 1 h, which increased to 41.6% ± 1.0% after 4 h of incubation (Fig. 2A) and a high internalization rate of above 95% (Supplemental Table 2). Binding of ^{99m}Tc-FAPI-19 was suppressed entirely by addition of 10^{-7} M unlabeled FAPI-19 (Fig. 2B), demonstrating the specificity and high affinity of this compound, with a half-maximal inhibitory concentration (IC_{50}) of 6.4 nM (Fig. 1). To ensure that the ^{99m}Tc chelator does not affect specificity, a binding experiment was conducted with 2 HEK cell lines transfected with either murine FAP (HEK-muFAP) or the closely related human membrane protein DPP4/CD26 (HEKCD26). Both murine FAP and CD26 show a high homology to human FAP (muFAP: 90% identity and 94% similarity on an amino acid level; CD26: 52% identity and 71% similarity with high structural resemblance) (*15*). As expected from previous experiments performed with DOTA-modified FAPI derivatives (*4,5*), we measured significant binding to murine FAP-expressing cells (36.13% ± 2.23%) after 60 min but almost no binding to CD26-expressing cells (0.2% ± 0.02%; Supplemental Table 3).

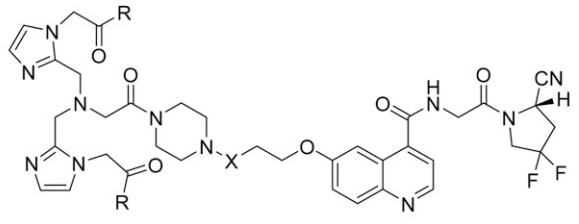

Name	X =	R =	IC_{50} [nM]
FAPI-19	-CH_2-	-OH	6.4
FAPI-28	-CH_2-	-L-Asn	12.7
FAPI-29	-CH_2-	-*N*-L-Glu	12.0
FAPI-33	-$(C_2H_4O)_2$-	-*N*-L-Glu	10.9
FAPI-34	-CH_2-	-*N*-L-Gla	6.9
FAPI-43	-CH_2-	-*N*-D-Arg	n.d.

FIGURE 1. FAPI derivatives for ^{99m}Tc labeling and corresponding IC_{50} values.

Because of the promising results, in vitro ^{99m}Tc-labeled FAPI-19 was investigated as an imaging agent in planar scintigraphy in a HT-1080-FAP–xenotransplanted mouse. As shown in Figure 3A and Supplemental Figure 3A, no tumor accumulation could be observed while the major portion of radioactivity was located in the liver. Besides a small fraction that was located in the bladder, the biliary elimination was observable by signals from the intestine after 30 min (Supplemental Fig. 3A). The circulating fraction was slightly detectable after 120 min and had vanished at 4 h, whereas a significant part of the activity was still located in the liver at 120 min and was recognizable therein 4 h after injection.

Suppression of Liver Accumulation and Hepatobiliary Excretion by Additional Hydrophilic Amino Acids

To improve the in vivo characteristics, the chelating moiety was modified with the amino acids Asn, Glu, and Gla (γ-carboxyglutamic acid). Additionally, a precursor with triethylene glycol as a spacer between the piperazinyl and quinolinyl moieties was synthesized to increase the hydrophilicity of the underlying FAPI-29 without further modification at the chelating moiety. Compared with the initially synthesized ^{99m}Tc-FAPI-19, the derivatives ^{99m}Tc-FAPI-33 and -34 revealed higher uptake ratios of up to 45.8% ± 1.3% and 41.86% ± 1.07%, respectively, on HT-1080-FAP cells (Fig. 2A). Furthermore, internalization rates above 95% (Fig. 2A; Supplemental Table 2) and high affinity for FAP, with IC_{50} values of 10.9 nM for FAPI-33 and 6.9 for FAPI-34, were observed (Fig. 1), as evaluated by competition experiments (Fig. 2B). In contrast, less binding was measured for ^{99m}Tc-FAPI-27 (≤12.94% ± 0.77%), ^{99m}Tc-FAPI-28 (≤37.52% ± 1.62%), ^{99m}Tc-FAPI-29 (≤39.34% ± 1.01%), and ^{99m}Tc-FAPI-43 (≤28.83% ± 0.88%) after exposure to HT-1080-FAP cells for 4 h (Fig. 2A). Furthermore, competition experiments revealed a slightly reduced affinity of these derivatives for FAP, with IC_{50} values of 12.0 nM for FAPI-29 and 12.7 nM for FAPI-28 (Fig. 1).

In Vivo Targeting Properties and Pharmacokinetics of ^{99m}Tc-Labeled FAPI Derivatives

To compare the in vivo targeting properties and pharmacokinetics of FAPI-28, -29, -33, -34, and -43 with those of FAPI-19 planar scintigraphy, biodistribution experiments on HT-1080-FAP–xenotransplanted mice were performed. The scintigraphic images demonstrated an improvement in the pharmacokinetics of the FAPI derivatives. Compared with FAPI-19 (Fig. 3A; Supplemental Fig. 3A), an accumulation of radioactivity in the tumor lesion and a reduction in the proportion of the hepatobiliary excretion was noticed at 60 min and lasted until at least 120 min after injection of the compounds (Fig. 3A). ^{99m}Tc-FAPI-34 showed the lowest uptake in the liver, biliary gland, and intestine

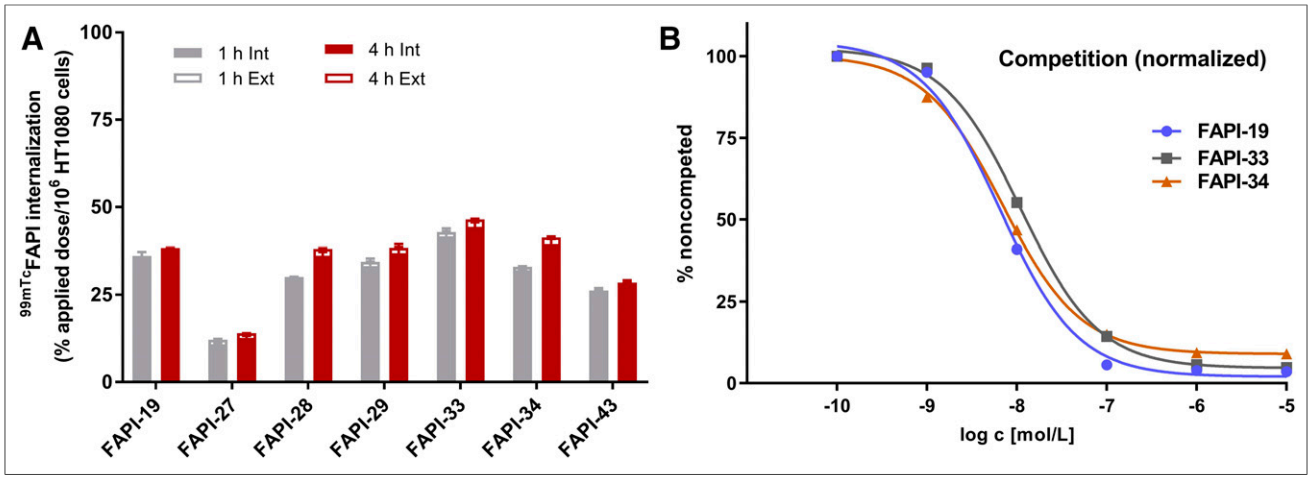

FIGURE 2. (A) Binding of ^{99m}Tc-labeled FAPI-19, -28, -29, -33, -34, and -43 to HT-1080-FAP. (B) Competitive binding of radiolabeled FAPI-19, -33, and -34 to HT-1080-FAP cells after adding increasing concentrations of corresponding unlabeled FAPIs. All values are given as percentage of total applied dose normalized to 1 million cells.

and significant uptake in the tumor lesions of mice (Fig. 3A; Supplemental Fig. 3B), which was prevented by simultaneous injection of the unlabeled analog and confirmed the target specificity of the compound (Fig. 3B).

In accordance with these results, biodistribution experiments with ^{99m}Tc-FAPI-34 revealed a tumor uptake of 5.4 ± 2.05 and 4.3 ± 1.95 %ID/g and a liver uptake of 0.91 ± 0.25 and 0.73 ± 0.18 %ID/g at 1 and 4 h, respectively, after injection of the tracer (Fig. 4A). Except for the kidneys, less than 1 %ID/g of the FAPI-34 activity was detected in the blood and organs of xenografts, accounting for tumor-to-tissue ratios above 1 (Fig. 4B). In contrast, we measured a lower tumor uptake of ^{99m}Tc-FAPI-29 (2.79 ± 1.19 and 1.43 ± 1.13 %ID/g) and of ^{99m}Tc-FAPI-43 (2.41 ± 0.34 and 2.57 ± 0.32 %ID/g) at 1 and 4 h, respectively, after tracer injection (Supplemental Fig. 4). The liver uptake of these derivatives, however, increased from 0.63 ± 0.06 to 1.73 ± 1.33 %ID/g (FAPI-29) or slightly decreased from 1.74 ± 0.28 to 1.56 ± 0.03 %ID/g (FAPI-43) after 1 and 4 h, respectively. In summary, ^{99m}Tc-FAPI-34 provided the best pharmacokinetics in xenografts and was, therefore, clinically applied for scintigraphy and SPECT.

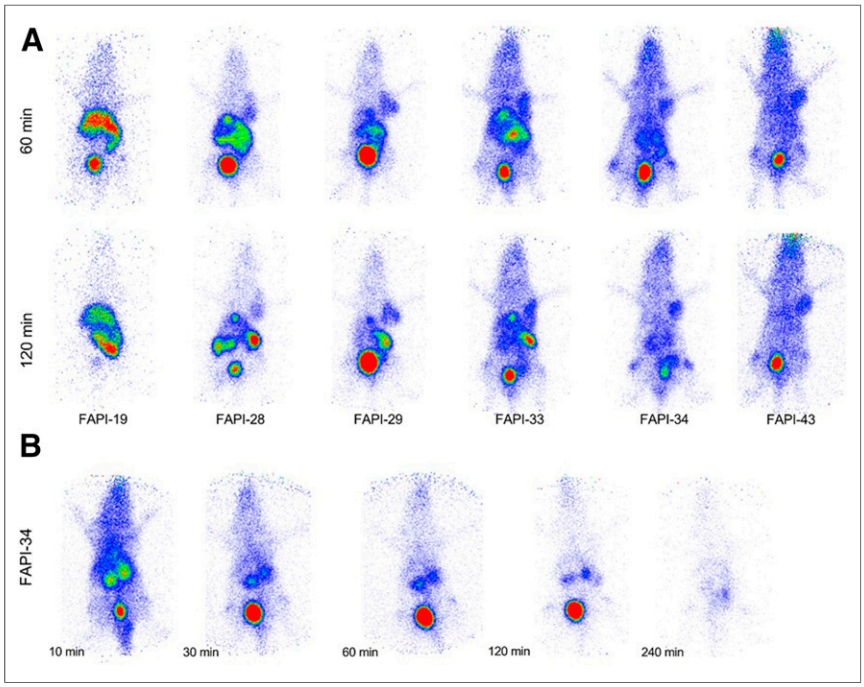

FIGURE 3. Planar scintigraphy of HT-1080-FAP tumor–bearing nude mice at 60 and 120 min after application of ^{99m}Tc-labeled FAPI derivatives (A) and at 10 min, 30 min, 1 h, 2 h, and 4 h after simultaneous injection of 30 nmol of unlabeled FAPI-34 used as competitor and ^{99m}Tc-FAPI-34 (B). Images are collected over 10 min at individual time points.

FAPI-34 Accumulation in Human Tumors

Two patients with metastasized ovarian and pancreatic cancer underwent PET with ^{68}Ga-FAPI-46, therapy with ^{90}Y-FAPI-46 in the setting of a last-line treatment, and scintigraphy or SPECT with ^{99m}Tc-FAPI-34. The patient with metastasized ovarian cancer underwent ^{68}Ga-FAPI-46 PET/CT on July 7, 2018, followed by therapy with 6 GBq of ^{90}Y-FAPI-46 on July 25, 2018. Therapy follow-up was done using ^{99m}Tc-FAPI-34 on September 19, 2018, and showed stable disease. The patient with pancreatic cancer had a previous FAPI therapy in June 2018. The ^{99m}Tc-FAPI-34 scintigraphy was done for follow-up. One day after scintigraphy, another therapy was done with 6 GBq of ^{90}Y-FAPI-46. Therapy was done with ^{90}Y because ^{188}Re was not available at that time. Six weeks later, follow-up imaging was done with FAPI-46 PET/CT. In both cases, the tumor lesions could be visualized (Figs. 5 and 6; Supplemental Figs. 5 and 6). Although evidence of a biliary secretion into the intestine was found in animal experiments, this was not the case in these patients.

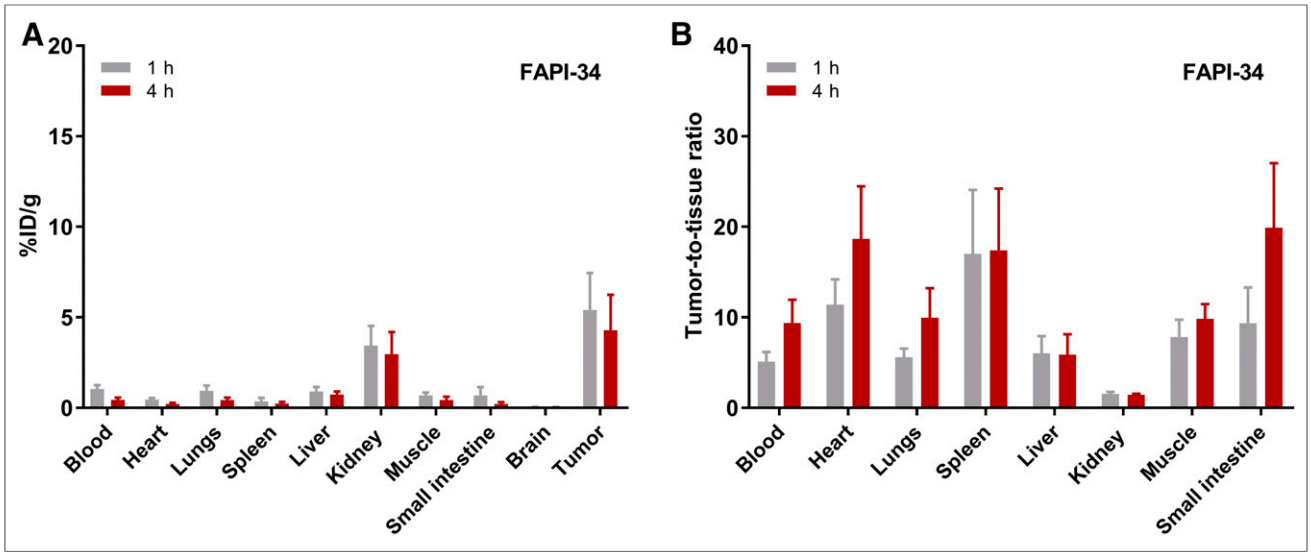

FIGURE 4. Biodistribution of ^{99m}Tc-FAPI-34 in HT-1080-FAP–xenotransplanted mice (A) and tumor-to-tissue ratios at 1 and 4 h after application of radiotracer (B). $n = 6$ for each time point.

DISCUSSION

The stromal component of tumors not only constitutes a major part of the tumor lesion but also is involved in many stroma–to–tumor-cell interactions such as signaling and remodeling of the extracellular matrix, which may lead to immunosuppression, resistance to chemotherapy, angiogenesis, tumor growth, and metastasis (*16–20*). Since cancer-associated fibroblasts are known to be important drivers of these reactions, the development of targeting strategies against these cells can be useful for diagnostic and therapeutic applications. In previous work, we described a couple of tracers based on inhibitors of the fibroblast activation protein (*21,22*). These were conjugated to DOTA, enabling radiolabeling with a variety of commonly available radionuclides for PET imaging and possibly also for endoradiotherapy (*4–8,11*).

To optimize the efficacy of FAPI-based endoradiotherapy, the physical half-life of the therapeutic radionuclide used for labeling has to be adjusted to the tumor retention time. Since FAPIs show a faster elimination out of the tumor than do other molecules, such as PSMA or somatostatin receptor ligands, ^{177}Lu or ^{225}Ac is not the ideal candidate for therapy with FAPIs. In contrast, ^{188}Re, a β-emitter with a half-life of 17 h, seems to be better suited. Therefore, FAPI variants with chelators dedicated to the binding of ^{99m}Tc and ^{188}Re were designed and evaluated in vitro and in vivo. Although all compounds displayed high-affine FAP-specific binding with IC_{50} values ranging from 6.4 to 12.7 nM and internalization of more than 95%, small-animal scintigraphy revealed different pharmacokinetic properties for the FAPI compounds. Compared with the primary molecule, FAPI-19, an improved tumor delineation was observed for FAPI-28, -29, -33, -34, and -43. The high lipophilicity of the tricarbonyl complex, as reported for PSMA ligands or somatostatin receptor–targeted compounds (*12,23*), causes a hepatobiliary elimination of FAPI-19 resulting in a lack of tumor accumulation. This fact may result from an unspecific binding of blood components such as lipoproteins, which overpowers the binding to FAP by inhibiting the conversion into the tumor tissue, accompanied by a fast deposition rate in the liver without an enterohepatic circulation. However, as shown in Supplemental Table 1, all FAPI compounds revealed a comparable plasma protein binding. Furthermore, the attachment of amino acids with hydrophilic side chains results in only small reductions in the logP value. In the case of arginine, the difference was most noticeable, whereas the value counterintuitively was raised in a substance with additional polar groups, which also performed better than the original FAPI-19. Therefore, other factors must be responsible for the differences in tumor uptake.

To enable renal excretion, 4 derivatives with higher hydrophilicity were designed and evaluated. Because of the availability of the building blocks and their biocompatibility, hydrophilic amino acids were chosen for the fine-tuning of the radiotracers. A first tumor accumulation was achieved by the attachment of asparagine with a neutral carboxamide side chain (FAPI-28). However, the introduction of glutamic acid (FAPI-29) and, thereby, a negatively charged carboxylate side chain even improved tumor accumulation and renal clearance of the radiotracer. Since peritoneal metastases, as well as liver cancers and metastases, are important for diagnosis, the accumulation in the intestine and liver had to be further minimized after enabling tumor targeting. Additionally, the slow hepatobiliary excretion would lead to a high nontarget organ dose representing a major drawback for the envisaged therapy with ^{188}Re. Arginine (FAPI-43) with a positively charged residue was also tested but was discarded because of the slow background clearance in scintigraphy.

Because of the promising results with glutamic acid, 2 alterations were tested to further improve the pharmacokinetic properties. One approach was the insertion of a triethylene glycol linker and the other was the application of carboxyglutamic acid, which carries an additional negatively charged carboxyl function. The PEG derivative FAPI-33 showed tumor accumulation and biliary excretion similar to that of FAPI-29, with a supposedly longer circulation in the blood pool as a result of the expected slower renal clearance caused by the higher hydrodynamic radius of PEG oligomers (*24*). In this series, FAPI-29 and FAPI-34 were identified as the compounds with the lowest background activity in scintigraphy. Therefore, FAPI-29 and FAPI-34 were used for biodistribution studies. Although FAPI-34 showed a slower uptake in

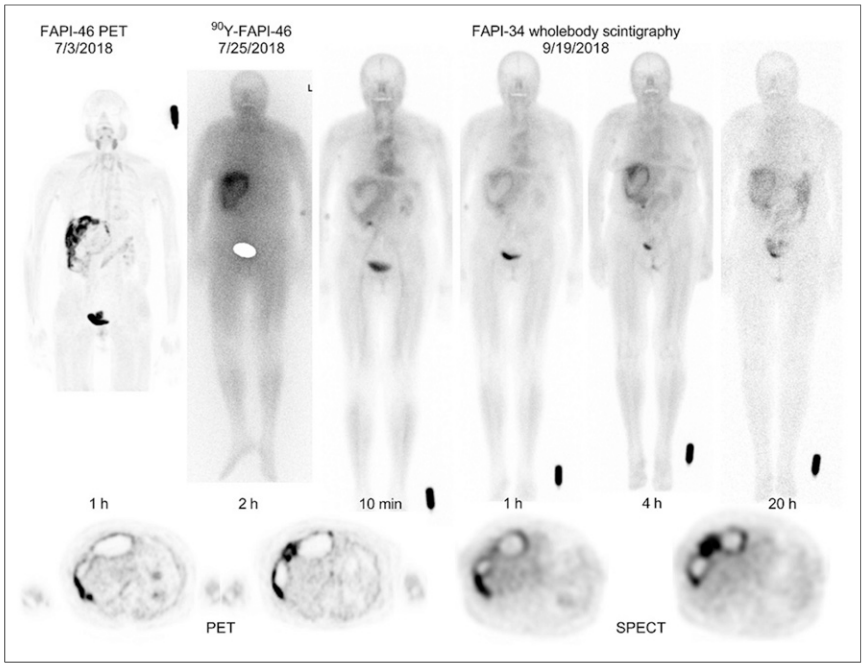

FIGURE 5. ^{68}Ga-FAPI-46 PET/CT (*11*) intratherapeutic imaging (Bremsstrahlung) during treatment with 6 GBq of ^{90}Y-FAPI-46 and scintigraphy with ^{99m}Tc-labeled FAPI-34 (planar scintigraphy and transaxial SPECT slices) in patient with ovarian cancer.

vitro, which might be caused by the 2 additional carboxyl functions, the in vivo performance of this compound in comparison to FAPI-29 could be improved. FAPI-34 revealed a stability in human serum over 4 h without noticeable degradation products (Supplemental Fig. 2), and a 2-fold and 8-fold higher tumor uptake at 1 and 4 h after injection, respectively. Liver uptake was comparable at 1 h but increased 2.7-fold for FAPI-29 at 4 h and remained stable for FAPI-34. Therefore, redistribution to the liver during hepatobiliary excretion, with decreasing tracer availability to the tumor, may be an explanation for the difference in tumor uptake. In view of the higher and constant tumor accumulation of FAPI-34 versus the lower and decreasing tumor uptake for FAPI-29, and the evidence obtained from the scintigraphy and biodistribution study that there is a hepatobiliary excretion route for FAPI-29, FAPI-34 was chosen for application in humans.

However, a difference in kidney uptake between scintigraphy and biodistribution was observed. This difference may originate from resting activity in the urine of the pelvic system after the animals are killed—that is, the difference between the in vivo situation in the small-animal SPECT scanner and the ex vivo situation during the biodistribution experiment. Consequently, the images obtained from 2 patients with metastasized cancer better resemble the small-animal PET, with radioactivity seen predominantly in the renal pelvis rather than the renal parenchyma, as was also observed with the ^{68}Ga-labeled FAPIs. The scintigraphic images corresponded largely to the images obtained by PET/CT. However, we have to admit that the PET/CT was 8 wk earlier and 5 wk later than the SPECT/CT in the patient with ovarian cancer and the patient with pancreatic cancer, respectively. This difference may be critical, especially in fast-growing tumors such as pancreatic and ovarian cancer, and therefore requires additional patients for whom the interval between PET/CT and SPECT is substantially shorter, that is, 4 wk at maximum.

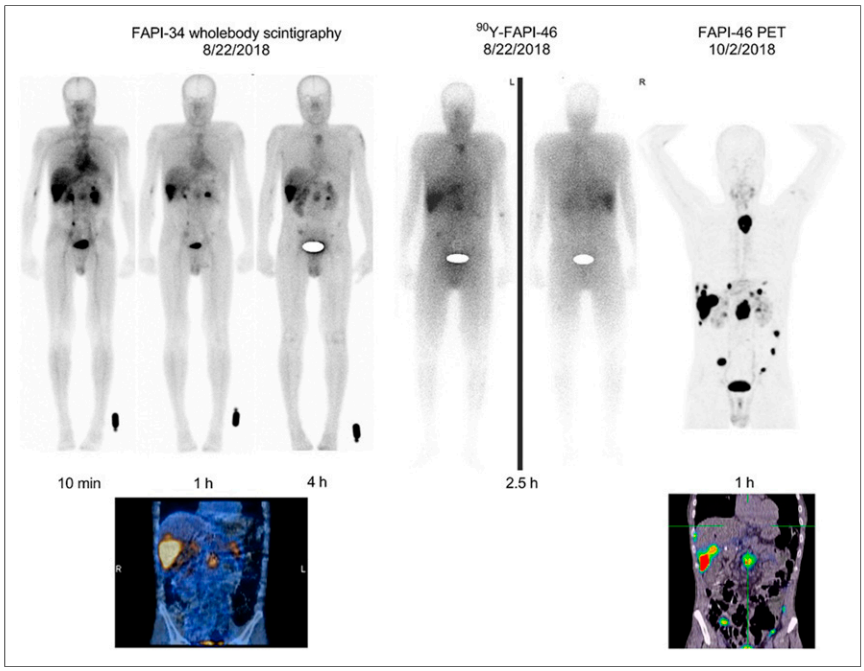

FIGURE 6. ^{99m}Tc-labeled FAPI-34 in planar scintigraphy and coronal SPECT fusion intratherapeutic imaging (Bremsstrahlung) during treatment with 6 GBq of ^{90}Y-FAPI-46 and ^{68}Ga-labeled FAPI-46 PET imaging (*11*) in patient with pancreatic cancer.

CONCLUSION

Although all compounds displayed high-affine FAP-specific binding, with IC_{50} values ranging from 6.9 to 13 nM and internalization of more than 95%, small-animal scintigraphy revealed different pharmacokinetic properties for the FAPI derivatives. Compared with the primary compound, FAPI-19, we observed improved tumor delineation for the FAPI-19 derivatives, which carry additional hydrophilic groups.

FAPI-34 may be a good candidate for scintigraphic imaging because of its high contrast obtained by rapid tumor uptake and fast clearance from the rest of the body. Since the chelator allows labeling with ^{188}Re, the tracer may also be applicable for endoradiotherapy of desmoplastic tumors with high FAP expression. However, this has to be

shown with data obtained in more patients and of course requires dosimetric calculations.

DISCLOSURE

Anastasia Loktev, Thomas Lindner, Walter Mier, Clemens Kratochwil, Frederik Giesel, and Uwe Haberkorn have a patent application (EP 18155420.5) for quinoline-based FAP-targeting agents for imaging and therapy in nuclear medicine. This work was funded in part by the Federal Ministry of Education and Research, grant 13N 13341. No other potential conflict of interest relevant to this article was reported.

ACKNOWLEDGMENTS

We thank Stefan Bauer (National Center for Tumor Diseases, Heidelberg) for supplying the FAP-α and CD26 transfected cell lines, and we thank Stephanie Biedenstein, Kirsten Kunze, Irina Kupin, Vanessa Kohl, Marlene Tesch, and Karin Leotta for providing excellent technical assistance.

KEY POINTS

QUESTION: Can a FAPI variant be established that can be used for scintigraphy and ^{188}Re endoradiotherapy?

PERTINENT FINDINGS: The systematic variation of the linker and chelator resulted in a SPECT tracer with high tumor uptake and low background uptake in animals and in first patient examinations.

IMPLICATIONS FOR PATIENT CARE: The new variant FAPI-34 shows promise for scintigraphic visualization and endoradiotherapy of FAP-positive tumors.

REFERENCES

1. Marsh T, Pietras K, McAllister SS. Fibroblasts as architects of cancer pathogenesis. *Biochim Biophys Acta.* 2013;1832:1070–1078.
2. Lamprecht S, Sigal-Batikoff I, Shany S, et al. Teaming up for trouble: cancer cells, transforming growth factor-β1 signaling and the epigenetic corruption of stromal naïve fibroblasts. *Cancers (Basel).* 2018;10:61.
3. Jiang G-M, Xu W, Du J, et al. The application of the fibroblast activation protein α-targeted immunotherapy strategy. *Oncotarget.* 2016;7:33472–33482.
4. Loktev A, Lindner T, Mier W, et al. A tumor-imaging method targeting cancer-associated fibroblasts. *J Nucl Med.* 2018;59:1423–1429.
5. Lindner T, Loktev A, Altmann A, et al. Development of quinoline-based theranostic ligands for the targeting of fibroblast activation protein. *J Nucl Med.* 2018;59:1415–1422.
6. Kratochwil C, Flechsig P, Lindner T, et al. ^{68}Ga-FAPI PET/CT: tracer uptake in 28 different kinds of cancer. *J Nucl Med.* 2019;60:801–805.
7. Giesel F, Kratochwil C, Lindner T, et al. ^{68}Ga-FAPI PET/CT: biodistribution and preliminary dosimetry estimate of 2 DOTA-containing FAP-targeting agents in patients with various cancers. *J Nucl Med.* 2019;60:386–392.
8. Giesel FL, Heussel CP, Lindner T, et al. FAPI-PET/CT improves staging in a lung cancer patient with cerebral metastasis. *Eur J Nucl Med Mol Imaging.* 2019;46:1754–1755.
9. Lindner T, Loktev A, Giesel F, Kratochwil C, Altmann A, Haberkorn U. Targeting of activated fibroblasts for imaging and therapy. *EJNMMI Radiopharm Chem.* 2019;4:16.
10. Zimmerman CN, Babich JW, Joyal J, Marquis J, Wang JC, inventors; Molecular Insight Pharmaceuticals Inc., assignee. Selective Seprase Inhibitors. U.S. patent US20100098633A1.
11. Loktev A, Lindner T, Burger EM, et al. Development of fibroblast activation protein-targeted radiotracers with improved tumor retention. *J Nucl Med.* 2019;60:1421–1429.
12. Lu G, Maresca KP, Hillier SM, et al. Synthesis and SAR of ^{99m}Tc/Re-labeled small molecule prostate specific membrane antigen inhibitors with novel polar chelates. *Bioorg Med Chem Lett.* 2013;23:1557–1563.
13. Fischer E, Chaitanya K, Wuest T, et al. Radioimmunotherapy of fibroblast activation protein positive tumors by rapidly internalizing antibodies. *Clin Cancer Res.* 2012;18:6208–6218.
14. Wilson AA, Jin L, Garcia A, DaSilva JN, Houle S. An admonition when measuring the lipophilicity of radiotracers using counting techniques. *Appl Radiat Isot.* 2001;54:203–208.
15. Kelly T. Fibroblast activation protein-alpha and dipeptidyl peptidase IV (CD26): cell-surface proteases that activate cell signaling and are potential targets for cancer therapy. *Drug Resist Updat.* 2005;8:51–58.
16. Plava J, Cihova M, Burikova M, Matuskova M, Kucerova L, Miklikova S. Recent advances in understanding tumor stroma-mediated chemoresistance in breast cancer. *Mol Cancer.* 2019;18:67.
17. Puré E, Lo A. Can targeting stroma pave the way to enhanced antitumor immunity and immunotherapy of solid tumors? *Cancer Immunol Res.* 2016;4:269–278.
18. Bussard KM, Mutkus L, Stumpf K, Gomez-Manzano C, Marini FC. Tumor-associated stromal cells as key contributors to the tumor microenvironment. *Breast Cancer Res.* 2016;18:84.
19. Erdogan B, Webb DJ. Cancer-associated fibroblasts modulate growth factor signaling and extracellular matrix remodeling to regulate tumor metastasis. *Biochem Soc Trans.* 2017;45:229–236.
20. Gascard P, Tlsty TD. Carcinoma-associated fibroblasts: orchestrating the composition of malignancy. *Genes Dev.* 2016;30:1002–1019.
21. Jansen K, Heirbaut L, Cheng JD, et al. Selective inhibitors of fibroblast activation protein (FAP) with a (4-quinolinoyl)-glycyl-2-cyanopyrrolidine scaffold. *ACS Med Chem Lett.* 2013;4:491–496.
22. Jansen K, Heirbaut L, Verkerk R, et al. Extended structure–activity relationship and pharmacokinetic investigation of (4-quinolinoyl)glycyl-2-cyanopyrrolidine inhibitors of fibroblast activation protein (FAP). *J Med Chem.* 2014;57:3053–3074.
23. Maresca KP, Marquis JC, Hillier SM, et al. Novel polar single amino acid chelates for technetium-99m tricarbonyl-based radiopharmaceuticals with enhanced renal clearance: application to octreotide. *Bioconjug Chem.* 2010;21:1032–1042.
24. Kang JS, DeLuca PP, Lee KC. Emerging PEGylated drugs. *Expert Opin Emerg Drugs.* 2009;14:363–380.